SPATIO-TEMPORAL VERSUS TEMPORAL CHAOS IN A SPATIALLY EXTENDED MAGNETIC DYNAMICAL SYSTEM* **

J.J. ŻEBROWSKI AND A. SUKIENNICKI

Institute of Physics, Warsaw University of Technology
Koszykowa 75, 00-662 Warszawa, Poland

(Received December 28, 1992)

Nonlinear dynamical states of a spatially extended micromagnetic system — the Bloch wall — were analyzed by means of spatio-temporal diagrams and power spectral analysis in the spatial frequency domain. The system studied exhibits chaotic dynamics with propagating coherent spatial structures — Bloch lines — which have soliton properties. Although it is spatially extended only temporal chaos occurs. The symptoms of this type of chaos (spatially complex patterns changing violently with the time) in such a spatially extended system should not be confused with chaos in the space and the time simultaneously. The system is not spatially chaotic due to the existence in it of coherent spatial structures with a fixed length scale (kink solitons). In particular, the spatio-temporal diagrams certainly look complicated enough but spatial power spectra show only a low number of modes at a given time.

PACS numbers: 05.45. +b, 75.10. Hk, 75.60. Ch

1. Introduction

Deterministic chaotic dynamics is a fast growing field of research. One of the outstanding features of this field is the universality of the nonlinear phenomena seen in various systems. Thus, physically completely different systems may reach the state of chaotic dynamics by the same route (*e.g.* the period doubling route, intermittency or the Ruelle–Takens route [1] to name but three). The same universality allows the use of a number of very

* Presented at the V Symposium on Statistical Physics, Zakopane, Poland, September 21–30, 1992.

** This work was supported by KBN Grant no 2 0250 91 1.

potent tools of analysis in various systems having a very different physics. Liapunov exponents, fractal dimensions, return maps and $f(\alpha)$ curves have now been accepted as standard, although sometimes difficult, tools [2].

Most of the mentioned tools were initially devised and tested for discrete time systems (maps) or for systems described by ordinary differential equations. Spatially extended systems — the models for which have to be described by partial differential equations — may have a higher complexity. Specifically, it is not quite straightforward whether the Takens delay time phase trajectory reconstruction method [3] based on a single time series taken from an arbitrarily chosen spatial location within the system is always applicable to such systems. Recently, a number of authors have focussed attention on the phenomenon of spatial intermittency [4], in which some parts of the systems exhibit laminar regions and other parts exhibit turbulent behavior. For such systems, taking data for delay time reconstruction from different region should yield different results (see *e.g.* [5]). It has been also demonstrated [6] that information about a local perturbation flows through a spatially extended system with a certain propagation velocity and that the correlation between points of spatially extended system may decay with distance [7].

In this context, it has become increasingly important to understand which dynamical states of spatially extended nonlinear systems are spatially homogeneous and exhibit chaos in the time domain only. Opposed to these states would be such which display spatio-temporal chaos. In most of the research done on this aspect, connected maps were used [8] as models for spatially extended systems. Kaneko has developed a group of tools — spatio-temporal diagrams and the associated quantitative measures [9] — specifically in order to discern spatio-temporal chaos from chaos only in the time domain. Some of these tools have been applied to a partial differential system by Kosiński [10].

We have analyzed a spatially extended micromagnetic system — a magnetic domain wall of the Bloch type (Fig. 1). This system has been studied in the past in several contexts [11] and is described by a pair of nonlinear partial differential equations which can be derived from the Landau–Lifshitz–Gilbert equation [14]. Although the Bloch wall — by the textbook definition — has a finite width but is infinite along its surface, in the model which we are studying it is finite in one direction (its height) as if it were confined by the surfaces of a thin film [12]. The Bloch wall, when moving in a constant drive field larger than a critical magnitude (the Walker field [12]), has a large sensitivity to initial conditions and kink-soliton like structures (Bloch lines — Fig. 1) propagate along it [11–13]. We show that, because of the solitary wave like properties of the kinks, the complex patterns observed in the spatio-temporal diagrams are misleading and are only the effect of

temporal chaos in a spatially extended system. Power spectral analysis in the spatial domain shows that the structure is quasi-periodic in space (low number of modes). How generic is this property is also discussed.

2. Equations of motion

The equations of motion of the Bloch wall are [12, 15]:

$$\dot{q} = \gamma\Delta\left[2\pi M \sin(2\varphi) - \frac{2A\partial^2\varphi}{M\partial z^2}\right] + \alpha\Delta\dot{\varphi}$$

$$\dot{\varphi} = \gamma\left[H_z + \frac{2A}{\Delta M}\frac{\partial^2 q}{\partial z^2}\right] - \alpha\frac{\dot{q}}{\Delta}$$

$q(z,t)$ is the position of wall, $\varphi(z,t)$ is the azimuthal angle between magnetization and the wall surface, H_z the spatially uniform and constant in time drive field, α is the phenomenological damping constant, γ is the gyromagnetic ratio, $4\pi M$ is the saturation magnetization, A is the exchange constant, $\pi\Delta$ is the Bloch wall width.

Only numerical solutions of these equations are possible [12]. Because using the Fast Fourrier Transform algorithm properly requires a large number of spatial grid points — the full implicit scheme (for details see [16]) devised by Kosiński was used with 460 spatial grid points and an 0.2 ns time step.

3. Dynamical properties of the Bloch wall

The Bloch wall in a thin film of magnetic material with uniaxial perpendicular anisotropy (Fig. 1) has the following properties [11–13]:

- The dynamical mode of the motion of the wall depends on the magnitude of the drive field H_z,
- for H_z greater than the Walker critical field H_w (a characteristic of the magnetic material [15]) the specific mode of motion of the wall depends on a combination of the drive field magnitude and of the height h of the wall:
- for a given value of the drive (here: set to 12 Oe *i.e.* 1.08 Oe above the critical field H_w), depending on the value of the height h of the wall, periodic or chaotic states of the wall with coherent spatial structures — Bloch lines (Fig. 1) — occur (see also [11–13]).

For the purpose of this study the following states were analyzed:

- a periodic state at $h = 3$ μm
- chaotic states at $h = 3.5$, 5, 6, 12, 20, 30, and 40 μm.

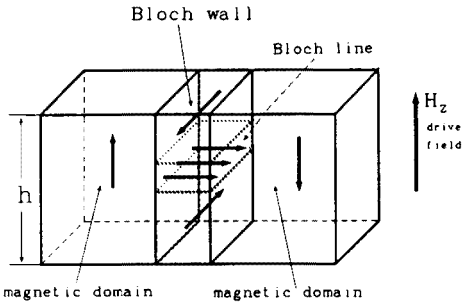

Fig. 1. The Bloch wall with a single horizontal Bloch line between two magnetic domains in thin film of a magnetic material with uniaxial perpendicular anisotropy.

The periodic state and the first three chaotic states have been studied previously [12, 14]. The states for larger wall height h were analyzed for the first time.

One or several coherent spatial structures — Bloch lines (Fig. 1) are present in the wall during the motion of the Bloch wall in any one of the states studied. Their number depends on the state but is, in general, greater when height of the wall is increased. Soliton properties of the coherent spatial structures of the Bloch wall [13] are an important feature of the system.

4. Spatio-temporal diagrams

The spatio-temporal diagrams were obtained by switching the pixel on when the difference between the value of the variable plotted and the spatial average of this variable at the given time was larger than a threshold value (0.1 — white, 1E-7 — gray) and positive. Every second spatial grid point was plotted (230 points for each variable) every time step (0.2 ns). This allowed the plotting of the spatio-temporal diagrams for both variables $\varphi(z,t)$ and $q(z,t)$ on the top and bottom, respectively, of a single screen of EGA 640×480 resolution.

5. Power spectral analysis

After the transients had died out, data for the spatial power spectra were stored every 5 ns for 500 ns. The spectra were calculated using the FFT algorithm with 460 data points padded on the right with zeroes up to 512. A Blackmann–Harris 3-rd order window was used to enhance spectral resolution by lowering the power at the side lobes. With the number of points available, the bandwidth was large enough so that no anti-aliasing

was needed. On the other hand, the spatial frequency resolution Δf is proportional to the reciprocal of the height of the wall h. This created a problem with the states for which h was small (less than 20 μm) which was partially offset by the fact that the shape of the wall for these states was simpler (less modes in the spectrum).

It is reasonable to suppose that the means of the flow of information about the Bloch lines propagating along $\varphi(z,t)$ is the vibrations of the wall shape $q(z,t)$. Only power spectra for $q(z,t)$ will be discussed here.

6. Results

6.1. Periodic states

The Bloch wall moving in a constant drive field is known to exhibit a sequence of periodic states — with the height of the wall as control parameter — which ends with a transition to chaos with isolated periodic windows [12, 14].

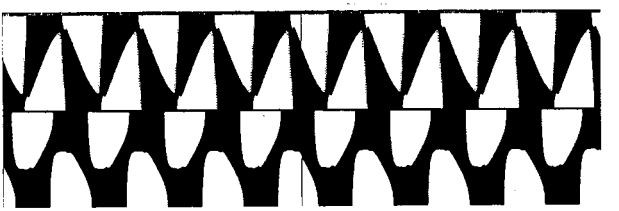

Fig. 2. Spatio-temporal diagram for $\varphi(z,t)$ (upper part) and $q(z,t)$ (lower part) for the periodic attractor at $h = 3.0$ μm for the time from 500 ns to 1011 ns. Position z is vertical and the time flows along the horizontal direction. Note that the dividing line in the middle of the graph is horizontal.

The spatio-temporal diagram for the state at wall height $h = 3.0$ μm (the last periodic state at the drive field $H_z = 12$ Oe before chaotic motion sets in [12, 14]) is shown in Fig. 2. It can be seen that the spatio-temporal pattern repeats itself regularly in time with all details of shape.

Spatial power spectral analysis for such a small height of the wall is difficult. Only a small part of a single period of the shape of the wall vibration is available to the FFT algorithm. Fig. 3 depicts eight typical examples of the spatial power spectra calculated for different values of time. Fig. 4 depicts a three-dimensional image of such power spectra for the time range 500–1000 ns calculated every 5 ns. From both of these figures it can be seen that individual spectra are harmonic with a single frequency

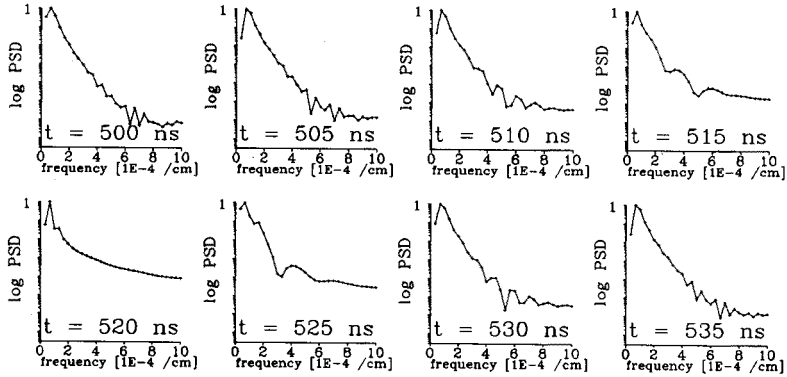

Fig. 3. Spatial power spectral density for eight values of the time calculated for the periodic attractor at $h = 3.0$ μm.

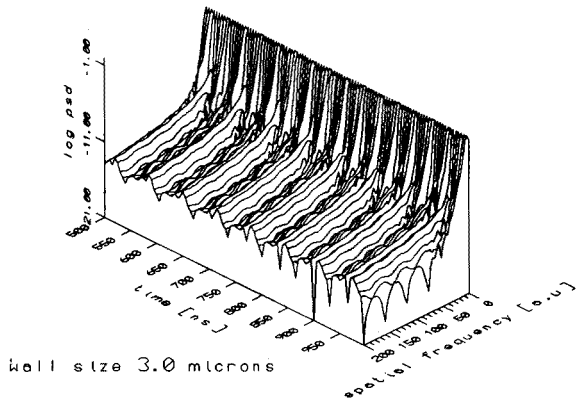

Fig. 4. Three-dimensional image of the spatial power spectra for the periodic attractor at $h = 3.0$ μm and for the time from 500 to 1000 ns.

dominating and that — although different for different time — they repeat periodically with the time.

6.2. Chaotic attractors

For comparison with the periodic states, the first chaotic state (for $h = 3.5$ μm) above the critical height at $h = 3.0$ μm was analyzed. The spatio-temporal diagram for this case is seen in Fig. 5. The eight examples of the power spectra are shown in Fig. 6 and the three-dimensional image

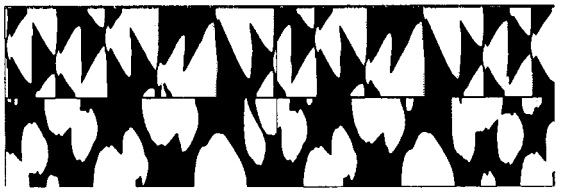

Fig. 5. Spatio-temporal diagram for $\varphi(z,t)$ (upper part and $q(z,t)$ (lower part) for $h = 3.5$ μm for the time from 500 ns to 1011 ns. Position z is vertical and the time flows along the horizontal direction.

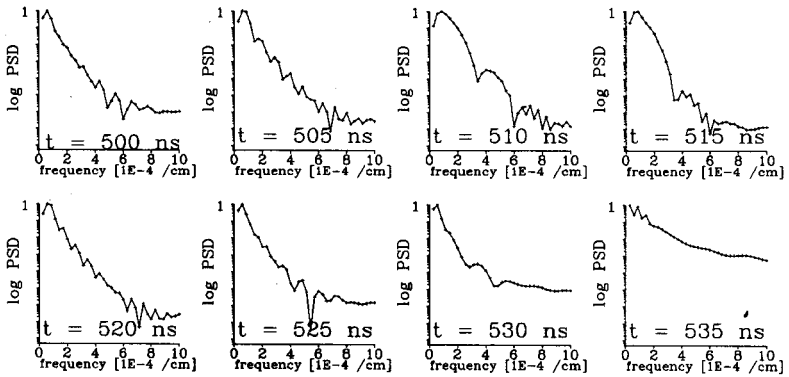

Fig. 6. Spatial power spectral density for eight values of the time calculated for the chaotic attractor at $h = 3.5$ μm.

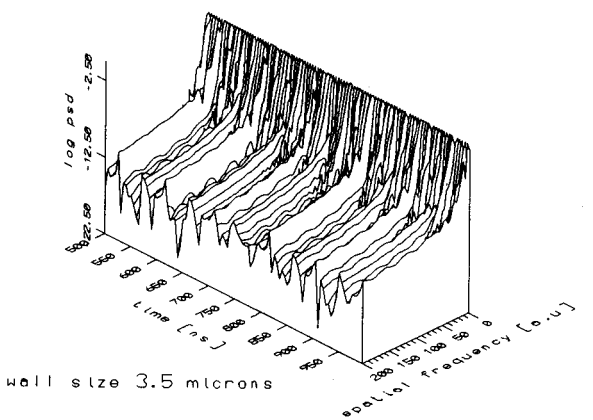

Fig. 7. Three-dimensional image of the spatial power spectra for the chaotic attractor at $h = 3.5$ μm and for the time from 500 to 1000 ns.

of the spectra calculated every 5 ns for the time range 500–1000 ns is shown in Fig. 7. Again the structure of the power spectra is harmonic with a single frequency dominating but in this the chaotic case there is no periodicity in the time. It was concluded then that this is the case of purely temporal chaos and that the very complexity of the spatio-temporal diagrams found for this state (and of the phase portraits — see Ref. [12, 14]) is just the result of a time average.

We calculated the spacial power spectra for other chaotic states (at $h = 4.5$ μm, 5.0 μm, 5.5 μm and 6.0 μm — discussed in our previous work [5, 12, 14]). All had the same feature in common: the structure of the spectra was harmonic and the bandwidth was limited. Characteristically, the modes represented in individual spatial spectra were different at different time. Again it was concluded that these are cases of temporal chaos. Note, that the attractor at $h = 5.0$ has been found to be spatially nonuniform [5, 14].

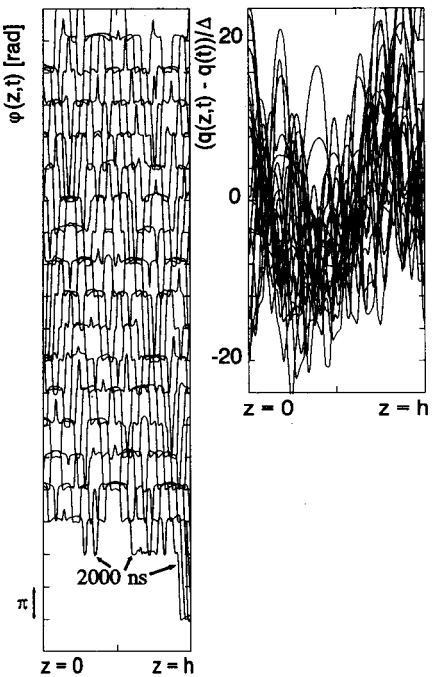

Fig. 8. Domain wall structure $\varphi(z,t)$ and wall shape $q(z,t)$ in a frame moving with the spatially averaged wall position $q(t)$ for $h = 40$ μm shown every 20 ns. The time range is from 2000 ns to 2450 ns. Δ is the Bloch wall width parameter.

The Bloch line width *i.e.* the width of the coherent spatial structures generated in the wall is of the order of 0.3 μm. Thus the aspect ratio for

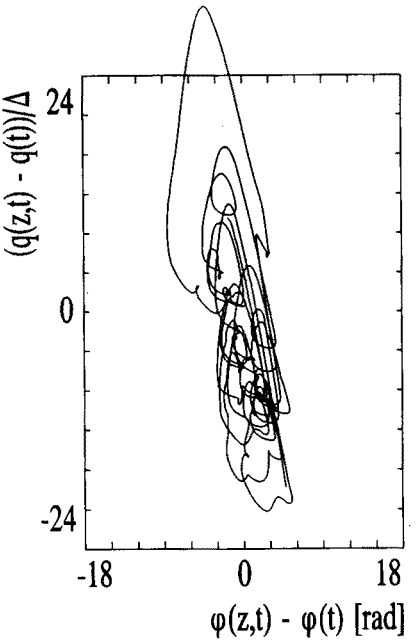

Fig. 9. Phase portrait for the midplane point in the wall for $h = 40$ μm. The time range is 2000 ns to 3000 ns.

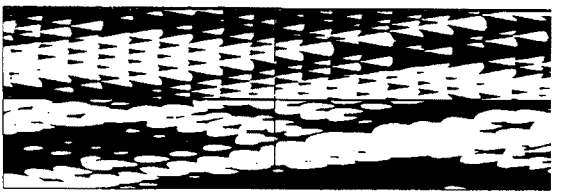

Fig. 10. Spatio-temporal diagram for $\varphi(z,t)$ (upper part) and $q(z,t)$ (lower part) for $h = 40$ μm for the time from 2000 ns to 2511 ns. Position z is vertical and the time flows along the horizontal direction.

the $h = 6.0$ μm is 20. In search of a truly spatially chaotic state we decided to increase the aspect ratio as much as possible. The largest height of the wall acceptable by our software (numerical accuracy) and by our hardware (memory limitations) was 40 μm (aspect ratio about 130). Fig. 8 depicts the time evolution of the structure $\varphi(z,t)$ and of the shape of the wall $q(z,t)$ (in a moving frame) for this case — after the transient has died out. The phase portrait of the midplane point of the wall may be seen in Fig. 9; this phase portrait reflects twice the evolution time range seen in Fig. 8. The spatio-temporal diagram for this attractor is seen in Fig. 10.

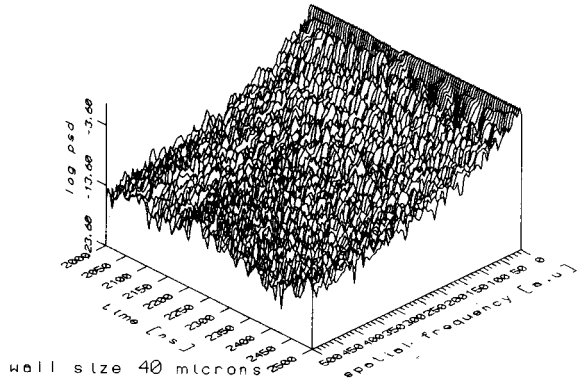

Fig. 11. Three-dimensional image of the spatial power spectra for the chaotic attractor at $h = 40$ μm and for the time from 2000 to 2500 ns.

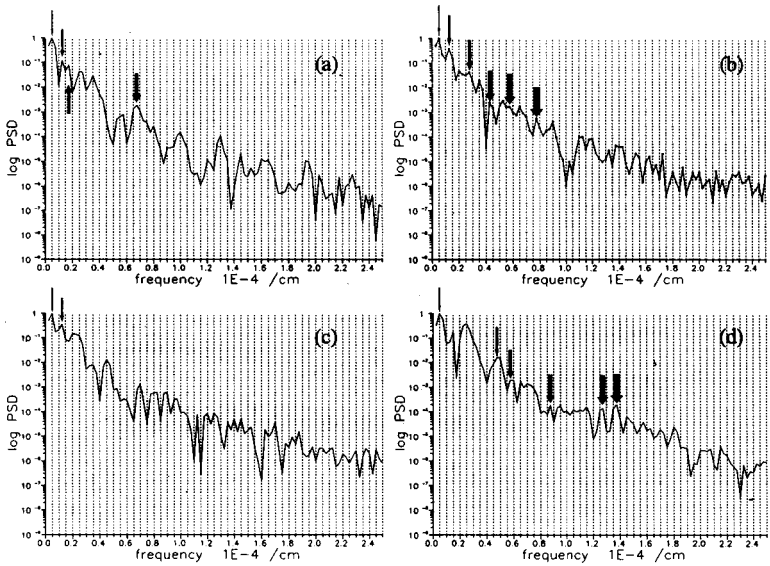

Fig. 12. Four examples of spatial power spectra for the attractor at $h = 40$ μm and the time $t = 2000$ ns (a), $t = 2040$ ns (b), $t = 2045$ ns (c) and $t = 2080$ ns (d). Basic modes marked by down arrows and linear combinations of modes by up arrows. Vertical dashed line indicates multiples of the spatial frequency of the strongest mode.

The complicated, nonperiodic pattern with small features appearing randomly and irregularly in time qualifies this state as a good candidate for spatio-temporal chaos. Indeed, the three-dimensional image of the spatial power spectra is certainly complicated (Fig. 11). However, careful analysis

of spatial power spectra for individual times shows that the state of the wall is still spatially quasiperiodic. Fig. 12 depicts several typical examples of spatial power spectra; it can be seen that the number of different modes present in the wall shape is low (not more than 6 — down arrows in Fig. 12) and that the complicated structure of the spectrum is due to a large number of harmonics of the basic modes and also to occasional linear combinations of the basic modes (up arrow in Fig. 12a).

The width of the Bloch line is proportional to the square root of the exchange constant. Consequently, one other way of changing the aspect ratio is to reduce this parameter. We analyze the dynamics of the Bloch wall of our model with the exchange constant reduced ten times (aspect ratio 410).

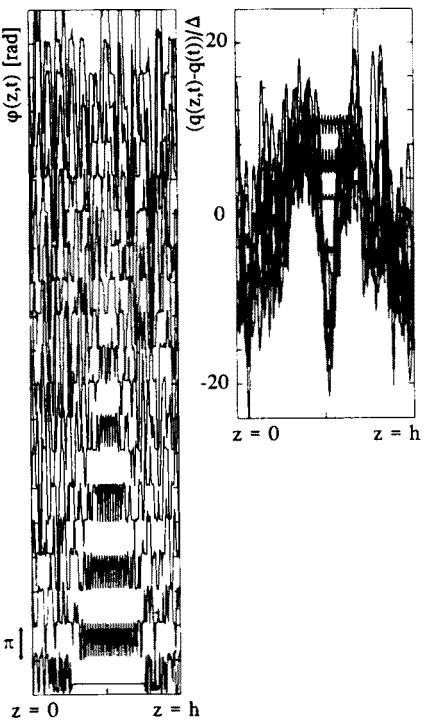

Fig. 13. Domain wall structure $\varphi(z,t)$ and wall shape $q(z,t)$ in a frame moving with the spatially averaged wall position $q(t)$ for the transient preceding the chaotic attractor at $h = 40$ μm and the tenfold reduced exchange constant — shown every 50 ns. The time range is from 250 ns to 750 ns. Δ is the Bloch wall width parameter.

During the transient phase the system behaves initially as if a kind of spatially chaotic state was reached. The time evolution of the structure

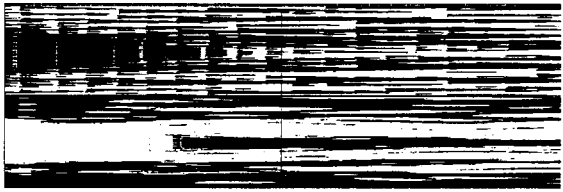

Fig. 14. Spatio-temporal diagram for $\varphi(z,t)$ (upper part) and $q(z,t)$ (lower part) for the transient preceding the chaotic attractor at $h = 40$ μm and tenfold reduced exchange constant — for the time from 251 ns to 762 ns. Position z is vertical and the time flows along the horizontal direction.

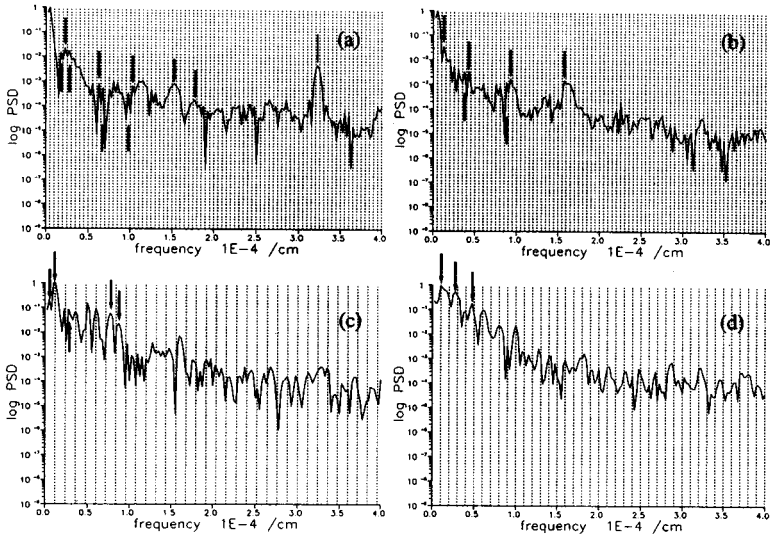

Fig. 15. Four examples of spatial power spectra for the transient preceding the attractor at $h = 40$ μm and the tenfold reduced exchange constant. The time $t = 260$ ns (a), $t = 305$ ns (b), $t = 450$ ns (c) and $t = 750$ ns (d). Basic modes marked by down arrows and linear combinations of modes by up arrows. Vertical dashed line indicates multiples of the spatial frequency of the strongest mode.

$\varphi(z,t)$ (Fig. 13) displays high frequency oscillations and the wall shape is suitably complicated. Also, the spatio-temporal diagram (Fig. 14) is composed of many small and seemingly randomly distributed islands. However, spatial frequency analysis shows that even in this transient phase the number of spatial modes is low (Fig. 15 — basic modes marked by down arrows and linear combinations of basic modes marked by up arrows). Also as time progresses, the high frequency mode visible in the initial stages of the transient (Fig. 15a) disappears (Fig. 16). Again, as in all previous chaotic cases analyzed, the specific modes present in the spectra at different times were different.

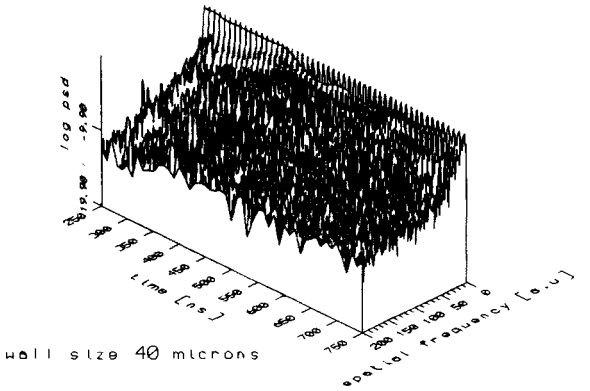

Fig. 16. Three-dimensional image of the spatial power spectra for the transient preceding the chaotic attractor at $h = 40$ μm and tenfold reduced exchange constant — for the time from 250 to 750 ns.

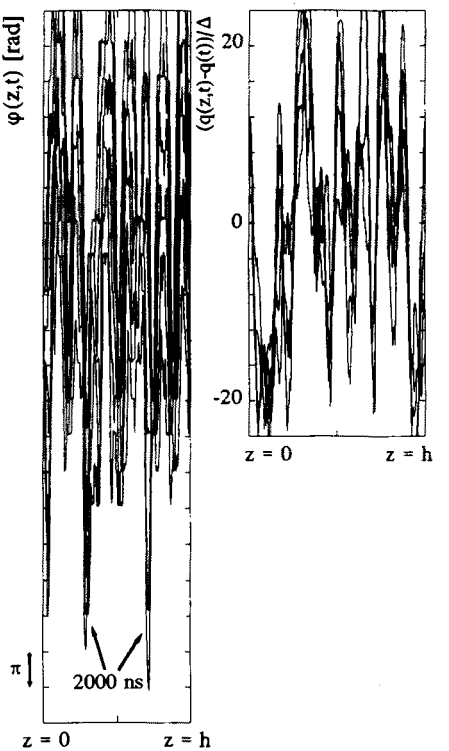

Fig. 17. Domain wall structure $\varphi(z,t)$ and wall shape $q(z,t)$ in a frame moving with the spatially averaged wall position $q(t)$ for the chaotic attractor at $h = 40$ μm and tenfold reduced exchange constant — shown every 50 ns. The time range is from 250 ns to 450 ns. Δ is the Bloch wall width parameter.

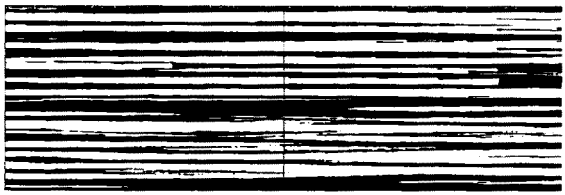

Fig. 18. Spatio-temporal diagram for $\varphi(z,t)$ (upper part) and $q(z,t)$ (lower part) for $h = 40$ μm and tenfold reduced exchange constant — for the time from 2001 ns to 2562 ns. Position z is vertical and the time flows along the horizontal direction.

After the transient has died out, the Bloch wall adopts — for the aspect ratio 410 — a new mode of motion. For all cases studied up to now [11–14], the change of the average angle $\varphi(t)$ — necessary for the wall to move [11, 14] — was realized by lateral motion of the Bloch lines. With the exchange constant decreased tenfold, at the end of the transient phase the wall structure develops large stacks of Bloch lines of up to 20 π-kinks each (Fig. 17). The mode of motion is then to grow new pairs of kink-antikink at the high points of the $\varphi(z,t)$ curve and simultaneously annihilate kink-antikink pairs at the low points of the curve. The over all effect reminds one visually of a viscous finger flow. The spatio-temporal diagram for this case is shown in Fig. 18 and seems to indicate that this state is spatio-temporal chaos. However, spatial frequency analysis seems to show otherwise. The number of frequency modes in the spectra for individual times is low (less than six) (Fig. 19) and this time many of the modes are long lived (Fig. 20).

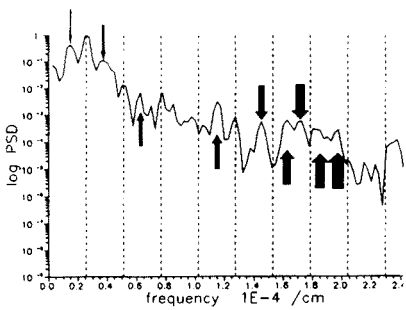

Fig. 19. An example of the spatial power spectrum for the chaotic attractor at $h = 40$ μm and tenfold reduced exchange constant — for the time $t = 2000$ ns. Basic modes marked by down arrows and linear combinations of modes by up arrows. Vertical dashed line indicates multiples of the spatial frequency of the strongest mode.

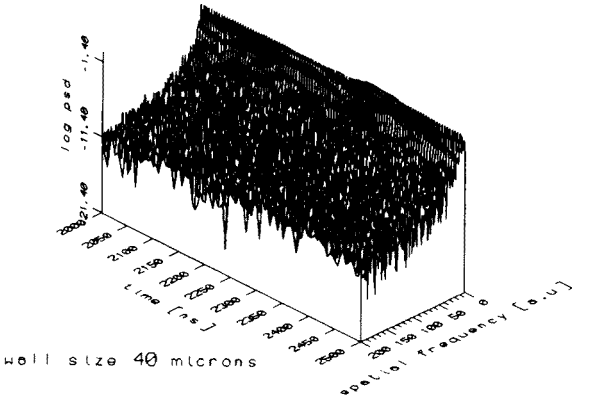

Fig. 20. Three-dimensional image of spatial power spectra for the chaotic attractor at $h = 40$ μm and tenfold reduced exchange constant — for the time from 2000 to 2500 ns.

7. Discussion and conclusions

We have analyzed the dynamics of a spatially extended dynamical system with coherent spatial structures. These structures are in the form of topologically stable π-kinks or stacks of π-kinks and play a major role in the dynamical states — both periodic and chaotic. By spatial frequency analysis of the state of the wall at different times, we found the chaotic states — even for a grossly large aspect ratio of 410 — to be quasiperiodic in space. The complex patterns observed in spatio-temporal diagrams were found to be in this sense misleading. We conclude then that the chaotic states found for our system are the result of temporal chaos alone which coexists with spatial quasiperiodicity.

The most important difference between our system and those modeled by coupled maps and also hydrodynamic systems is that in our system the coherent structures present have a minimum characteristic length scale — the width of the single π-kink (Bloch line). Thus, the cascade of states with ever diminishing length scales which leads to a fully developed turbulence in hydrodynamics is impossible. What is also interesting is that, in our system, the low number of spatial frequency modes present at a given time seems to indicate a correlation between the relatively larger number of individual coherent spatial structures within the wall. It can be surmised that, in other systems, individual π-kinks may also "communicate" over distances much exceeding their width. This may happen through *e.g.* exchange of small amplitude (linear) vibrations. In such a system — as in ours — chaotic states would be the result of temporal chaos alone.

The authors gratefully acknowledge the use of the full implicit finite difference scheme for the solution of the equations of motion devised by dr Kosiński. Without this method, the generation of a sufficiently large number of data points for FFT analysis would have been impossible.

REFERENCES

[1] H.G. Schuster, *Deterministic Chaos — An Introduction*, Physik-Verlag, Weinheim 1988.

[2] A. Wolf, J. Swift, L. Swinney, *Physica* **D16**, 285 (1985); P. Szephalusy, T. Tel, A. Csordas, Z. Kovacs, *Phys. Rev.* **A36**, 3525 (1987); P. Grassberger, I. Procaccia, *Phys. Rev. Lett.* **50**, 5, 346 (1983).

[3] F. Takens, *Phys. Rev. Lett.* **51**, 14, 1265 (1980); A. Broomhead, G. King, in *Nonlinear Phenomena and Chaos*, Hilger, Bristol 1986.

[4] H. Chaté, P. Manneville, *Phys. Rev. Lett.* **58**, 112 (1987); P. Manneville, in *Experimental Study and Characterization of Chaos*, ed. Hao Bai-Lin, World Scientific, Singapore 1990.

[5] J. Żebrowski, submitted to *Phys. Rev.* **A**.

[6] P. Grassberger, *Phys. Scripta* **40**, 346 (1989); J.A. Vastano, H.L. Swinney, *Phys. Rev. Lett.* **60**, 1773 (1988).

[7] Y. Pomeau, *C.R. Acad. Sc. Paris* **300**, Série II, 7, 239 (1985); T. Kurz, G. Mayer-Kress, in *Lecture Notes in Physics* **278**, Springer, Berlin 1987; G. Mayer-Kress, T. Kurz, *Complex Systems* **1**, 821 (1987).

[8] J.P. Crutchfield, K. Kaneko, in *Directions in Chaos*, ed. Hao Bai-Lin, World Scientific, Singapore 1987.

[9] K. Kaneko, in *Dynamics and Statistics of Patterns*, ed. K. Kawasaki *et al.*, World Scientific, Singapore 1989.

[10] R.A. Kosiński, *Phys. Lett.* **A169**, 263 (1992).

[11] J. Żebrowski, A. Sukiennicki, *Acta Phys. Pol.* **A72**, 299 (1987); R.A. Kosiński, J. Żebrowski, A. Sukiennicki, *J. Phys. D* **22**, 451 (1989).

[12] J. Żebrowski, *Phys. Scripta* **38**, 632 (1988).

[13] J. Żebrowski, *Phys. Rev.* **B39**, 7205 (1989).

[14] J. Żebrowski, A. Sukiennicki, to appear in *Deformations of Mathematical Structures: Surface Effects*, ed. J. Ławrynowicz, Kluver 1993.

[15] A.P. Malozemoff, A.C. Slonczewski, *Magnetic Domain Walls*, American Press 1979.

[16] R.A. Kosiński, J. Engemann, *J. Magn. Magn. Mat.* **50**, 229 (1985).